# Experimental Tests on a Multilevel Converter for Grid-Connected Photovoltaic Systems

G. Grandi, D. Ostojic, C. Rossi

*Alma Mater Studiorum* - University of Bologna
Department of Electrical Engineering
Viale Risorgimento 2, 40136 - Bologna, Italy
Ph. +39 051 20 93571, Fax. +39 051 20 93588
gabriele.grandi@mail.ing.unibo.it

***Abstract*–A complete set of experimental tests on a novel conversion scheme for three-phase grid-connected photovoltaic (PV) generation systems is presented in this paper. The proposed scheme is based on two insulated strings of PV panels, each one feeding a standard two-level three-phase voltage source inverter (VSI). The inverters are connected to grid by a three-phase transformer with the open winding configuration on inverters side. The resulting conversion structure acts as a multilevel converter, doubling the power capability of a single VSI with given current rating. An original control method has been introduced to regulate the dc-link voltages of each VSI, allowing the whole converter to inject the PV energy into the grid and to perform as a power active filter.**

## I. INTRODUCTION

Because of constantly growing energy demand, grid-connected photovoltaic systems are becoming more and more popular, and many countries have permitted, encouraged, and even funded distributed power generation systems. Yet the technology presents shortcomings such are high initial installation cost and low energy conversion efficiency, requiring constant improvement of both cell and power converter technologies [1], [2].

The connection of the PV field to the ac grid is usually made with a voltage source inverter, and it may include intermediate dc/dc converters, transformers, or even both. In many countries national electric code requires transformer's presence to achieve galvanic insulation of panels with respect to the network. Even if topology includes transformer (either high- or line-frequency), the system with a dc/dc converter will operate over a wider input voltage range but with higher cost and lower conversion efficiencies at most operating points. Transformerless and high-frequency transformer topologies are preferred for omitting bulky LF transformer, but limited to single-phase output with powers up to few kW. The restrictions arise from switching losses and limited power of the HF magnetic components. Hence, PV converter with line-frequency transformer is prevailing in higher power range, i.e., from few tens of kW up to MW, contributed by the fact that LF transformer's cost per watt decreases as rated power increases.

The novel topology for PV grid-connected systems proposed by the Authors in [3], [4] (Fig. 1) has been recently implemented and the experimental results are given in this paper. The conversion system utilizes a dual inverter structure connected to open-end primary windings of a standard three-phase transformer. The PV field is shared into two equal PV fields. Each inverter can be directly coupled with one PV field, as shown in Fig. 1, or through dc/dc stage, an option available for all PV converters. The secondary windings are connected to the grid with traditional either delta or star configuration. Note that the transformer contributes with its leakage inductance to the ac-link inductance which is always necessary for the grid connection of a VSI. Furthermore, the presence of a low-frequency transformer enable the direct connection of high power generations system to the medium voltage grid (10-20 kV).

The resulting three-phase converter is able to operate as a multilevel inverter, with reduced harmonic distortion and lower dv/dt in the output voltages. The main advantage of this topology is the simplified hardware structure with respect to traditional multilevel inverters, increasing both the effectiveness and the reliability in medium- and high-power applications. Also, it can use standard six-transistor configuration readily available also as modules, without additional diodes and switches. A control algorithm with standard PI controllers is proposed to achieve commanded values of dc voltages necessary for maximum power point tracking (MPPT) of PV panels. Beside power generation the system can function as an active filter, with the additional capabilities of load balancing, harmonics compensation and reactive power injection.

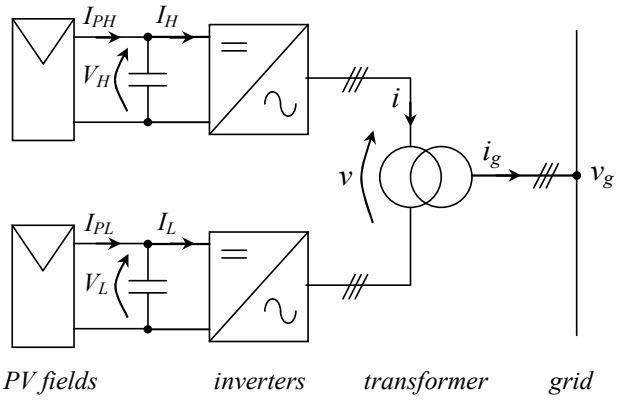


Fig. 1. Proposed dual-inverter configuration.

## II. Dual Inverter Topology

Three-level inverters are a good tradeoff solution between performance and cost in multi-level converter for both medium and high-power applications. The main advantages of three-level inverters are reduced voltage ratings for the switches, good harmonic spectrum (making possible the use of smaller and less expensive filters), and good dynamic response. In particular, the output voltage waveform of the converter has up to nine output levels of phase voltage. The dual two-level inverter structure (Fig. 1) gives the same output voltage as three-level inverter with a simple combination of standard three-phase VSI [5], [6]. Then, it represents a viable solution when the three-phase load can be connected in the open-winding configuration, as for transformers and ac motors, and especially when the dc source can be easily split in two insulated supplies, as for batteries and PV panels. Note that the presence of two insulated dc sources easily prevent the circulation of zero-sequence currents, avoiding the use of an additional homopolar reactor or the application of a modified voltage modulation algorithm which doesn't produce zero-sequence voltage but leads to lower dc bus voltage utilization [7].

In present case of PV applications, demanded dc voltage range can be directly obtained by adjusting the number of series-connected panels for each PV string. The MPPT action is performed by the inverters, regulating the dc-bus voltages, as explained in the following section. Another possibility is inclusion of intermediate dc/dc converters, which simultaneously take over role of MPP trackers, enabling optimal and constant dc voltages for the two inverters.

With reference to the scheme of Fig. 1, using space vector representation, the output voltage vector $\bar{v}$ of the multilevel converter is given by the contribution of the voltage vectors $\bar{v}_H$ and $\bar{v}_L$, generated by inverter H and L respectively [8]:

$$\bar{v} = \bar{v}_H + \bar{v}_L . \tag{1}$$

The combination of the eight switching configuration for each inverter yields total 64 switching states corresponding to 19 different output voltage vectors, including zero vector. The resulting hexagonal locus can be subdivided in two areas, as represented in Fig. 2: the inner hexagon and the outer belt [8]. In a grid-connected application voltage vector is always positioned in the outer belt, which means both inverters "H" and "L" have to contribute to the output voltage.

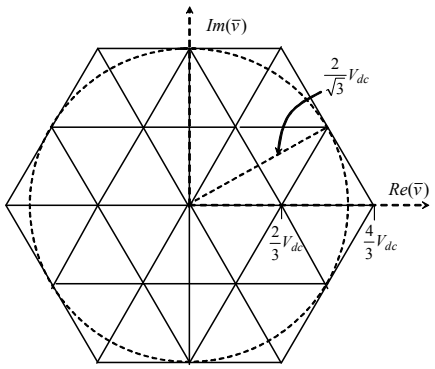


Fig. 2. Dual inverter voltage vector plot in the case $V_H = V_L = V_{dc}$.

## III. Converter Control

The conversion system is symmetric having both inverters with equal ratings and two equal groups (strings) of panels supplying them, i.e., the dc bus voltage reference, $V_{dc}^*$, is the same for both inverters. Nevertheless, two distinct voltage controllers have to be implemented to guarantee the system stability under unavoidable unsymmetrical characteristic or disturbances. The proposed control system is represented in the block diagram of Fig. 3.

The primary control task is voltage regulation of both PV strings to accomplish MPP for both of them. In the following, the voltage control is described in more detail while the MPP and other necessary supervisory tasks of the system control are not discussed further. It is important to note that control task is much more complex than in case of a single inverter configuration, because the proposed system is multivariable. While in single inverter configuration the only variable being controlled is ac current, in case of dual inverter ac current but also inverter's output ac voltages sharing between "H" and "L" inverters is influencing the state of the system.

The control algorithm utilized in this paper is based on simple PI controllers [3], [4]. The problem is somewhat similar to power sharing problem investigated in automotive applications, where proper multilevel voltage modulation strategy has been addressed [9]. In [10] the more complex approach of LQR techniques based on state-space models is considered.

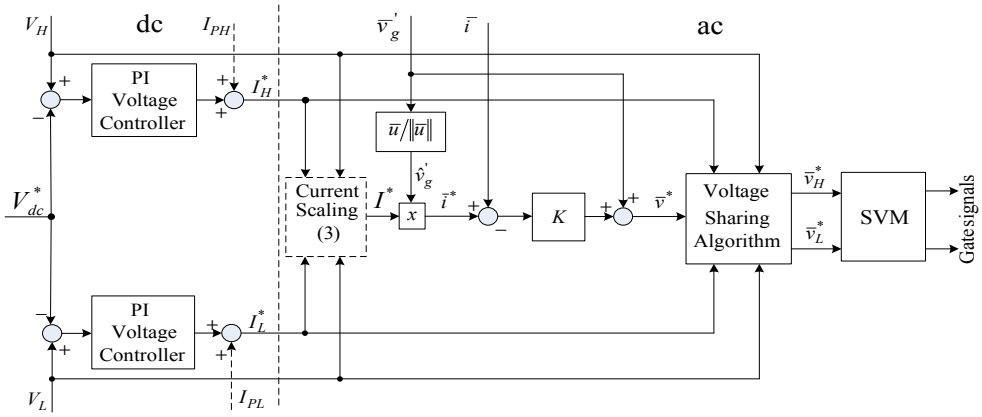


Fig. 3. Block diagram of proposed control system.

Another possibility is independent control of each inverter [11] but at the price of multilevel benefits loss.

The two dc voltages ($V_H$, $V_L$) are controlled by two proportional-integral controllers, giving as output the reference of two dc currents ($I_H^*$, $I_L^*$). A feed-forward action can be added in order to compensate sudden changes in PV currents ($I_{PH}$, $I_{PL}$), as shown in Fig. 3. Its utilization depends on the current transducer's availability and required dynamic response. The inverter output current reference is calculated based on power balance equation in steady-state. If the inverter current is injected into the grid in phase with the grid voltage, the power balance yields

$$V_H I_H + V_L I_L = 3 V_g' I \,, \tag{2}$$

where $V_g'$ is the grid voltage seen from the inverters' side (RMS) and $I$ is inverters' ac output current (RMS). Note that in (2) both inverter and transformer losses are neglected. Thus, current reference can be obtained from (2) as

$$I^* = \frac{1}{3}\frac{V_H I_H^* + V_L I_L^*}{V_g'} \,. \tag{3}$$

The current injected into the grid is assumed to be in phase with grid voltage, i.e. having only active component, as stated above. The resulting reference current space vector $\bar{i}^*$ for the converter is

$$\bar{i}^* = I^* \hat{v}_g \,, \tag{4}$$

being $\hat{v}_g$ the unity space vector of the grid voltage. It can be noted that reactive and/or harmonic compensation current references can be added if active power filter operating conditions are required.

To solve the known problem of current control in grid-connected application [12], simple P-controller with feed-forward action (grid voltage) has been chosen, due to its simplicity, good dynamic response and immunity to harmonic disturbance. Although it results in steady-state current error it is not a critical drawback since the controlled variable is dc voltage [3], [4]. In particular, the reference voltage $\bar{v}^*$ is here calculated as

$$\bar{v}^* = K(\bar{i}^* - \bar{i}) + \bar{v}_g' \tag{5}$$

being $\bar{v}_g'$ the space vector of the grid voltage seen from the inverters' side. The reference output voltage $\bar{v}^*$ can be synthesized as the sum of the voltages $\bar{v}_H^*$, $\bar{v}_L^*$ generated by the two inverters, as expressed by (1). Introducing the voltage ratio $k$ and imposing the inverter voltage vectors $\bar{v}_H^*$, $\bar{v}_L^*$ to be in phase with the output voltage vector $\bar{v}^*$, yields

$$\begin{cases} \bar{v}_H^* = k\,\bar{v}^* \\ \bar{v}_L^* = (1-k)\,\bar{v}^* \end{cases} \tag{6}$$

The condition expressed by (6) allows maximum voltage utilization. Furthermore, being $\bar{i}$ the same output current for both the two inverters, the coefficient $k$ also defines the power sharing between the two inverters, as follows (averaged values within the switching period):

$$p = \frac{3}{2}\bar{v}^* \cdot \bar{i} \;\; = p_H + p_L \quad \begin{cases} p_H = \frac{3}{2}\bar{v}_H^* \cdot \bar{i} \;\; = k \cdot p \\ p_L = \frac{3}{2}\bar{v}_L^* \cdot \bar{i} \;\; = (1-k) \cdot p \end{cases} \tag{7}$$

The coefficient $k$ has a limited variation range depending on the value of the reference output voltage $\bar{v}^*$, as investigated in [9]. An estimation of the coefficient $k$ is given by introducing a simple power balance, assuming $V_H \cong V_L \cong V_{dc}^*$:

$$k = \frac{p_H}{p} = \frac{V_L I_L}{V_L I_L + V_H I_H} \cong \frac{I_H}{I_L + I_H} \tag{8}$$

As a consequence, the individual inverter reference voltages $\bar{v}_H^*$, $\bar{v}_L^*$ can be determined on the basis of the following equations

$$\bar{v}_H^* = \frac{I_H^*}{I_H^* + I_L^*}\bar{v}^* \,,\; \bar{v}_L^* = \frac{I_L^*}{I_H^* + I_L^*}\bar{v}^* \,. \tag{9}$$

Further, it has to be provided that both references are within range of achievable output voltage of particular inverter, which depends on their dc voltages. This is an issue on which this topology differs from case of a single inverter topology: when the voltage demand exceeds available dc voltage there is a simple saturation. For the dual inverter configuration, total voltage reference must be satisfied, so in case of voltage saturation of one inverter the second has to make up the missing part. This problem is addressed in [4].

Once the inverter reference voltages $\bar{v}_H^*$ and $\bar{v}_L^*$ are determined, the modulation algorithm will ensure their application to transformer open-end windings. Generally, all pulse-width modulators for dual inverter can be divided in two groups. The first uses two independent modulators for two single inverters [11]. This approach is characterized by simplicity and large degree of freedom, but it fails to product proper multilevel waveform and consequently output include higher harmonic and ripple content. The second group contains composite modulators, which are able to produce proper multilevel voltage. Same as in the case of single inverter, there are carrier based (CB) and space vector (SV) PWMs. The earliest proposed CB modulation was with two phase-shifted sawtooth carriers [6]. Another CB modulation can be directly derived from the phase disposition multilevel modulation, with two triangular level-shifted carriers. Finally, a space vector PWM has been proposed [13]. Unfortunately all mentioned algorithms are based on symmetry of two single inverters voltages, and cannot provide proper multilevel output in case of different references. Since two references do not have to be necessarily equal in general it needs particular algorithm to provide proper multilevel voltage output [8], [9].

## IV. Simulation Results

The simulation model of the proposed topology and control scheme represented in Figs. 1 and 3 was implemented in MATLAB-Simulink, with modulator realized as C MEX S-function. The component ratings used for model are based on real laboratory prototype used for experimental tests. The PV panels have been electrically represented by the fitted V-I characteristic of a parallel arrangement of "*Solar Shelf*" SP150 modules. The main characteristics of the whole PV generation system prototype are summarized in Table I. Reference is made to the scheme presented in Fig. 1, with the PV panel strings directly connected to the inverters. In this case, the MPPT regulation is achieved by the change of inverters' dc bus voltage reference $V_{dc}^*$. The simulation results are presented in Figs. 4 and 5.

In the first case, Fig. 4, the voltage reference decreases with a step change from 37 V to 25 V, approximately corresponding to the change between open-circuit voltage and MPP voltage, introducing a sudden increment of the PV generated power. The change is chosen to be big and fast in order to test ability of the control system. Fig. 4 (a) shows the time behavior of dc voltage and dc current for both the inverters. It can be seen that the system response is very good since steady-state is reached within one period of grid voltage (20 ms) and without overshoot. A faster response could be achieved at the price of longer settling time. Another interesting point that can be observed is that currents $I_H$ and $I_L$ are noticeably different at the beginning of transient although both groups consist of equal number of panels with the same type. But since the start of the transient corresponds to no-load (or close to no-load) condition, when currents are close to zero, unavoidable small difference in currents leads to high relative differences. This can be concluded from (9) as well, converging to undetermined value as both numerator and denominator are closing to zero. Unavoidable small differences between $I_H$ and $I_L$ result with big change of their ratio. Described problem is a little of interest in practice, since

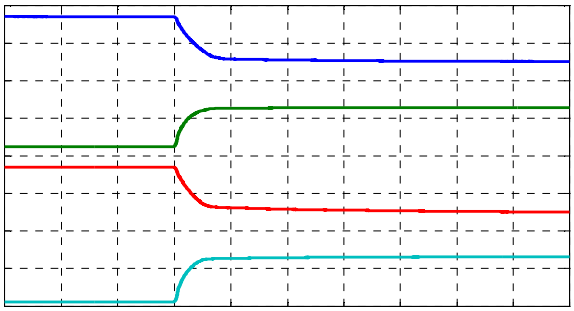

(a) dc voltage (10 V/div) and dc current (20 A/div) for both inverters, $V_H$, $I_H$, $V_L$, $I_L$ (from top to bottom).

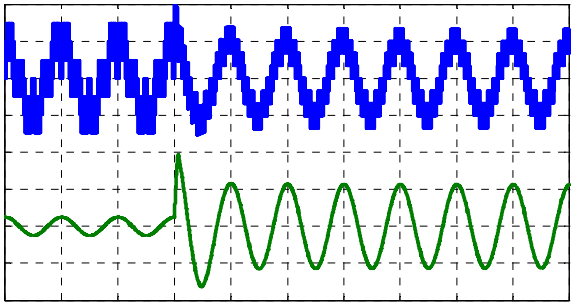

(b) converter ac voltage (25 V/div) and ac current (20 A/div).

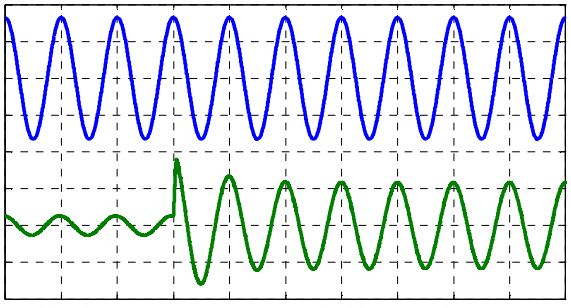

(c) grid voltage (upper, 200 V/div) and grid current (lower, 2 A/div).

Fig. 4. Step change (decrease) of the reference dc voltage, $V_{dc}^*$ (20ms/div)

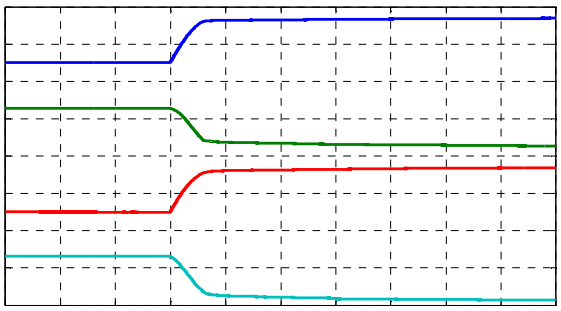

(a) dc voltage (10 V/div) and dc current (20 A/div) for both inverters, $V_H$, $I_H$, $V_L$, $I_L$ (from top to bottom).

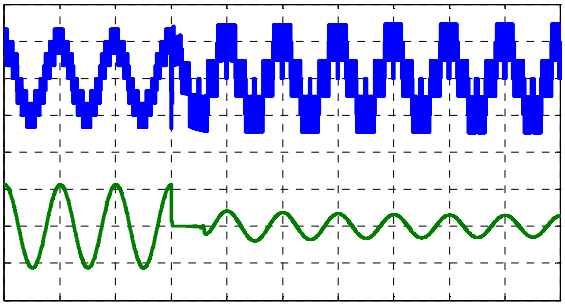

(b) converter ac voltage (25 V/div) and ac current (20 A/div).

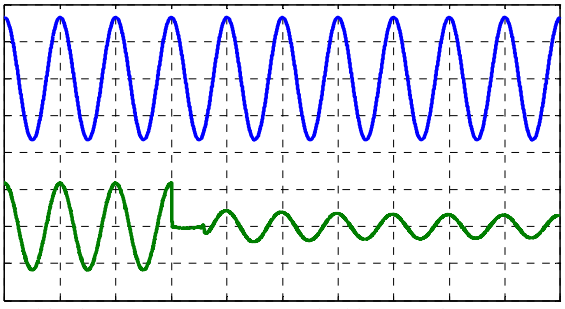

(c) grid voltage (upper, 200 V/div) and grid current (lower, 2 A/div).

Fig. 5. Step change (decrease) of the reference dc voltage, $V_{dc}^*$ (20ms/div)

system is controlled by MPPT algorithm governing operating point always far from no-load condition.

The output of the dual inverter (ac voltage and ac current) during the transient is shown in Fig. 4 (b). Proper voltage multilevel operation is achieved, and the current ripple is very small. An increase of modulation index due to the lower available dc voltage can be noted, as output changes from seven- to nine-level. The current is very slightly lagging the voltage because of the leakage inductors and transformer reactive power demand. Fig. 4 (c) shows that grid voltage (line-to-neutral) and grid current are in phase, as expected. The grid voltage waveform does not change during the transient, since it is set by the ac network, whereas the current amplitude increases in response of the sudden change of the PV generated power. It can be noted that for grid connected application producing only active power MPP corresponds to the operating point with maximum grid current amplitude. In the second case, Fig. 5, the voltage reference increases with a step from 25 V to 37 V, introducing a sudden decrement of PV generated power. Fig. 5 (a) shows the time behavior of dc voltage and dc current for both the inverters. Also in this case, the system response is good and steady state is reached in few ac periods, without overshoot. The output of the dual inverter (ac voltage and ac current) during the transient is shown in Fig. 5 (b). In this case, a decrease of modulation index due to the higher available dc voltage can be noted. Fig. 5 (c) shows grid voltage and grid current. The transient affects only the grid current amplitude, as stated above. Since the reference change is directly opposite to the previous one, the resulting values of voltages and currents correspond to the ones obtained in previous simulation, just in opposite order. In both Fig. 5 (b) and (c) an interval with very small ac current can be noticed. This is a consequence of the limit applied to (9), which permits only one direction of active power (to grid, but not from grid), in simple way avoiding possible problems with denominator equal to zero. As the result the settling time in this case is slightly higher than in previous case (Fig. 6).

## V. Experimental Tests

To ensure the safety, the system has been implemented by using only parallel connections of PV panels, since the presence of a grid-transformer with the proper turn ratio enables voltage adaptation. The resulting PV string voltage is around 30-40 V, allowing use of low-voltage MOSFETs. These types of switches are cheap, being widely used in automotive applications, and they feature good efficiency, since their on-state resistance is a strong decreasing function of the blocking voltage rating.

The main characteristics of the whole PV generation system prototype are summarized in Table I. Reference is made to the scheme presented in Fig. 1, with the PV panel strings directly connected to the inverters. In this case, the MPPT regulation is achieved by the change of inverters' dc bus voltage reference $V_{dc}^{*}$. A picture of the experimental set-up is shown in Fig. 6. The control algorithm is implemented in TMS320F2812 digital signal processor. The preliminary experimental tests show the dynamic behavior of the system in response to a step change of the dc voltage reference, $V_{dc}$*, simulating the action of a MPPT algorithm, not included in the present version of the paper.

In the first case, the voltage reference decreases with a step change from 37 V to 25 V, thus making the same transient as already analyzed in simulation (Fig. 4). The experimental results are shown in Fig. 7, and they completely correspond to previously shown in Fig. 4. It can be noticed that the response speed is slightly lower with respect to the simulation results. This can be due to the uncalculated parasitic resistances and voltage drops.

In the second case, Fig. 8, the voltage reference increases with a step from 25 V to 37 V, introducing a sudden decrement of PV generated power, corresponding to case analyzed in simulation (Fig. 5). Figure 8 (a) shows the time behavior of dc voltage and dc current for both the inverters. Also in this case, the system response is good and steady state is reached in few ac periods, without overshoot. The output of the dual inverter (ac voltage and ac current) during the transient is shown in Fig. 8 (b). In this case, a decrease of modulation index due to the higher available dc voltage can be noted. Fig. 8 (c) shows grid voltage and grid current. The obtained results show good agreement both with the previous

Table I
System Model and Prototype Characteristics

| 2 PV panel strings: Shell Solar SQ150-C (6 in parallel) | | | | |
|---|---|---|---|---|
| Grid transformer | | | Converter | |
| single-phase, 50 Hz | 3x | | three-phase VSI | 2x |
| rated voltages (V) | 24/400 | | IRF2807 (parallel MOSFETs) | 6x |
| rated power (VA) | 500 | | rated dc voltage (V) | 50 |
| short circuit voltage (%) | 6.9 | | rated ac current (A) | 240 |
| | | | switching freq. (kHz) | 20 |
| ac-link inductance (mH) | 0.4 | | dc-bus capacitance (mF) | 26 |

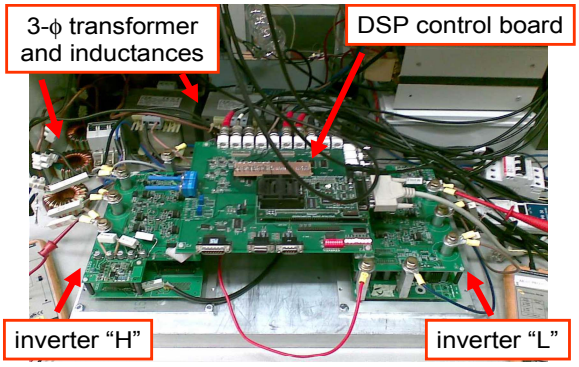

Fig. 6. Experimental set-up

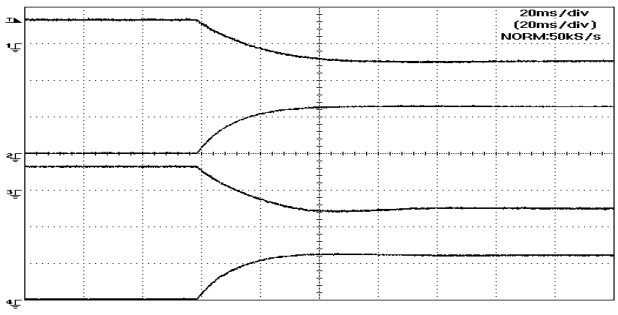


(a) dc voltage (10 V/div, 30 V offset) and dc current (20 A/div) for both inverters, $V_H$, $I_H$, $V_L$, $I_L$ (from top to bottom).

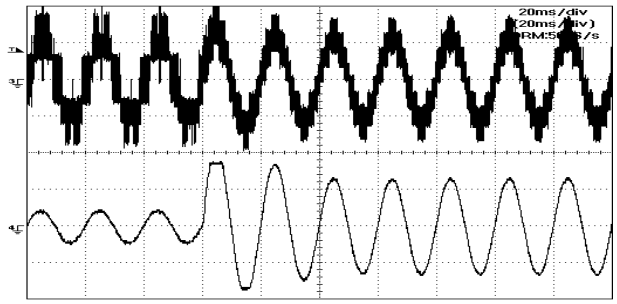

(b) converter ac voltage (25 V/div) and ac current (20 A/div).

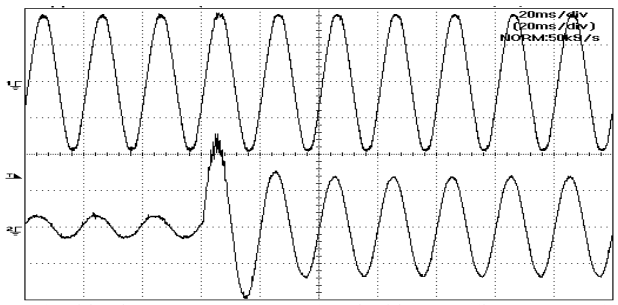

(c) grid voltage (upper, 200 V/div) and grid current (lower, 2 A/div).

Fig. 7. Step change (decrease) of the reference dc voltage, $V_{dc}^{*}$.

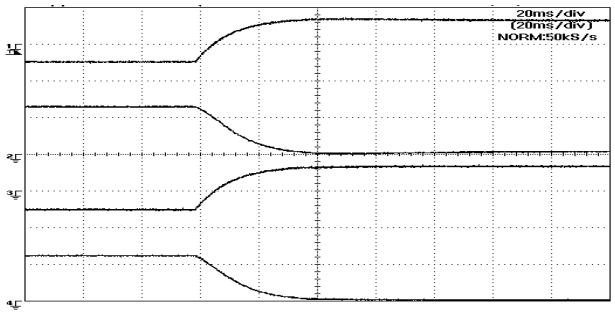


(a) dc voltage (10 V/div, 30 V offset) and dc current (20 A/div) for both inverters, $V_H$, $I_H$, $V_L$, $I_L$ (from top to bottom).

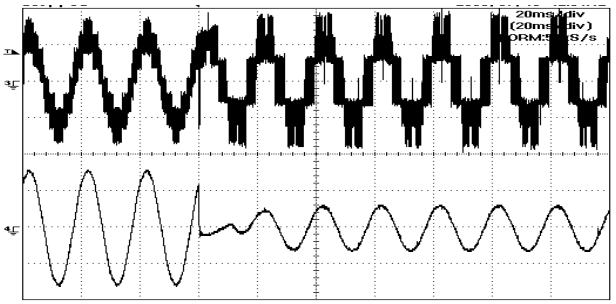

(b) converter ac voltage (25 V/div) and ac current (20 A/div).

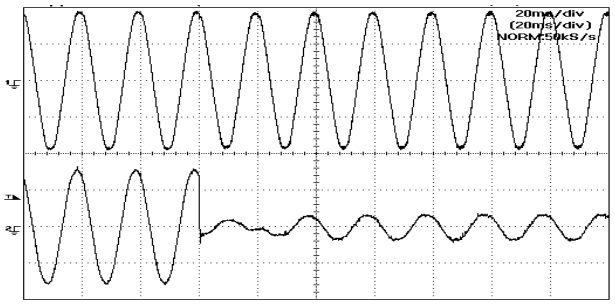

(c) grid voltage (upper, 200 V/div) and grid current (lower, 2 A/div).

Fig. 8. Step change (increase) of the reference dc voltage, $V_{dc}^{*}$.

experiment (Fig. 7) and with simulation results (Fig. 5). The slight difference can be noted in the short interval when current reference is saturated to zero, where can be noticed existence of small but non-zero current. This is probably due to the magnetizing current of the transformer.

## VI. Conclusion

A conversion topology for the grid connection of a photovoltaic generation system is analyzed and tested in this paper. The converter utilizes a dual inverter structure to extend rated maximum power and to realize multilevel ac voltage waveforms on the basis of standard three-phase inverters. The topology includes two insulated PV strings and a three-phase open-winding transformer. A simple and effective control algorithm has been implemented, including MPPT, providing power generation with unity power factor. The whole PV generation system has been realized and verified by both numerical simulations and experimental tests, showing good performance both in steady state and transient conditions.

## References

[1] S. Kjaer, J. Pedersen, F. Blaabjerg, "A Review of Single-Phase Grid-Connected Inverters for Photovoltaic Modules," *IEEE Trans. Industry Applications*, Vol. 41, No. 5, Sep 2005, pp. 1292-1306.

[2] T. Shimizu, M. Hirakata, T. Kamezawa, and H. Watanabe, "Generation control circuit for photovoltaic modules," *IEEE Trans. on Power Electronics*, Vol. 16, No. 3, May 2001, pp. 293-300.

[3] G. Grandi, D. Ostojic, C. Rossi, "Dual Inverter Configuration for Grid-Connected Photovoltaic Generation Systems," *Proc. 29th Int. Tel. En. Conf., INTELEC*, Sept. 30 –Oct. 4, 2007, Rome, Italy, pp. 880-885.

[4] G. Grandi, D. Ostojic, C. Rossi, D. Casadei, "Multilevel Power Conditioner for Grid-Connected Photovoltaic Applications," *14th IEEE Mediterranean Electrotechnical Conf.*, May 5-7, 2008, Ajaccio, France, pp. 573-578.

[5] I. Takahashi and Y. Ohmori, "High-performance direct torque control of an induction motor," *IEEE Trans. Industry Applications*, Mar. 1989, vol. 25, no. 2, pp. 257-264.

[6] H. Stemmler and P. Guggenbach, "Configurations of high-power voltage source inverter drives," in *Proc. Power El. and App. Conf.*, 1993, vol.5, pp. 7-14.

[7] M. Baiju, K. Mohapatra, R. Kanchan, K. Gopakumar, "A dual two-level inverter scheme with common mode voltage elimination for an induction motor drive," *IEEE Trans. on Power Electronics*, vol. 19, No. 3, May 2004, pp. 794-805.

[8] D. Casadei, G. Grandi, A. Lega, C. Rossi, L. Zarri, "Switching technique for dual-two level inverter supplied by two separate sources", *Applied Power Electronics Conference and Exposition, APEC*, Anaheim, California (USA), Feb. 25 - Mar. 1, 2007, pp.1522-1528.

[9] G. Grandi, C. Rossi, A. Lega, D. Casadei, "Multilevel operation of a dual two-level inverter with power balancing capability," *Proc. of IEEE Industry Applications Soc. Annual Meeting, IEEE-IAS*, Tampa, Florida (USA), Oct. 8 - 12, 2006.

[10] S. Alepuz, S. Busquets-Monge, J. Bordonau, J. Gago, D. Gonzalez, J. Balcells, "Interfacing Renewable Energy Sources to the Utility Grid Using a Three-Level Inverter," *IEEE Trans. on Industrial Electronics*, vol. 53, no. 5, Oct. 2006, pp. 1504-1511.

[11] J. Kim, J, Jung, K, Nam, "Dual-inverter control strategy for high-speed operation of EV induction motors," *IEEE Trans. on Industrial Electronics*, vol. 51, no. 2, Apr. 2004, pp. 312- 320.

[12] F. Blaabjerg, R. Teodorescu, M. Liserre, A.V. Timbus, "Overview of Control and Grid Synchronization for Distributed Power Generation Systems," *Trans. on Ind. El.*, vol. 53, no. 5, pp. 1398-1409, Oct. 2006.

[13] E. G. Shivakumar, K. Gopakumar et al., "Space vector PWM control of dual inverter fed open-end winding induction motor drive," *Proc. of 16th IEEE Applied Power Electronics Conf.*, Anaheim, 2001, pp. 399-405.